MATERIALS SCIENCE

D. B. Sirdeshmukh
L. Sirdeshmukh
K. G. Subhadra

Micro- and Macro-Properties of Solids

Thermal, Mechanical and Dielectric Properties

Springer

Springer Series in
MATERIALS SCIENCE 80

Springer Series in

MATERIALS SCIENCE

Editors: R. Hull R. M. Osgood, Jr. J. Parisi H. Warlimont

The Springer Series in Materials Science covers the complete spectrum of materials physics, including fundamental principles, physical properties, materials theory and design. Recognizing the increasing importance of materials science in future device technologies, the book titles in this series reflect the state-of-the-art in understanding and controlling the structure and properties of all important classes of materials.

71 **Dissipative Phenomena in Condensed Matter**
Some Applications
By S. Dattagupta and S. Puri

72 **Predictive Simulation of Semiconductor Processing**
Status and Challenges
Editors: J. Dabrowski and E.R. Weber

73 **SiC Power Materials**
Devices and Applications
Editor: Z.C. Feng

74 **Plastic Deformation in Nanocrystalline Materials**
By M.Yu. Gutkin and I.A. Ovid'ko

75 **Wafer Bonding**
Applications and Technology
Editors: M. Alexe and U. Gösele

76 **Spirally Anisotropic Composites**
By G.E. Freger, V.N. Kestelman, and D.G. Freger

77 **Impurities Confined in Quantum Structures**
By P.O. Holtz and Q.X. Zhao

78 **Macromolecular Nanostructured Materials**
Editors: N. Ueyama and A. Harada

79 **Magnetism and Structure in Functional Materials**
Editors: A. Planes, L. Mañosa, and A. Saxena

80 **Micro- and Macro-Properties of Solids**
Thermal, Mechanical and Dielectric Properties
By D.B. Sirdeshmukh, L. Sirdeshmukh, and K.G. Subhadra

81 **Metallopolymer Nanocomposites**
By A.D. Pomogailo and V.N. Kestelman

82 **Plastics for Corrosion Inhibition**
By V.A. Goldade, L.S. Pinchuk, A.V. Makarevich and V.N. Kestelman

83 **Spectroscopic Properties of Rare Earths in Optical Materials**
Editors: G. Liu and B. Jacquier

84 **Hartree–Fock–Slater Method for Materials Science**
The DV–X Alpha Method for Design and Characterization of Materials
Editors: H. Adachi, T. Mukoyama, and J. Kawai

85 **Lifetime Spectroscopy**
A Method of Defect Characterization in Silicon for Photovoltaic Applications
By S. Rein

86 **Wide-Gap Chalcopyrites**
Editors: S. Siebentritt and U. Rau

87 **Micro- and Nanostructured Glasses**
By D. Hülsenberg and A. Harnisch

88 **Introduction to Wave Scattering, Localization and Mesoscopic Phenomena**
By P. Sheng

Volumes 20–70 are listed at the end of the book.

D.B. Sirdeshmukh
L. Sirdeshmukh
K.G. Subhadra

Micro- and Macro-Properties of Solids

Thermal, Mechanical and Dielectric Properties

With 209 Figures and 153 Tables

Springer

Professor D.B. Sirdeshmukh
Professor L. Sirdeshmukh
Professor K.G. Subhadra
Kakatiya University
Physics Department
Warangal 506 009, India
E-mail: dsirdeshmukh@yahoo.com

ISSN 0933-033X

ISBN-10 3-540-31785-6 Springer Berlin Heidelberg New York

ISBN-13 978-3-540-31785-2 Springer Berlin Heidelberg New York

Library of Congress Control Number: 2006928433

Typesetting: Data prepared by the Authors and by SPi using a Springer TEX macro package
Cover concept: eStudio Calamar Steinen
Cover production: *design & production* GmbH, Heidelberg

Printed on acid-free paper SPIN: 11554769 57/3100/SPi 5 4 3 2 1 0

To the memory of our mentors

Prof. R. Satyanarayan
Prof. V.T. Deshpande
Prof. P.G. Puranik
Prof. K. Venkata Ramaiah

Preface

This book deals with some micro and macroproperties of solids. Microproperties are perceived at the lattice level and are generally studied by diffraction or spectroscopic methods. The lattice constant, its temperature variation (measured through the property of thermal expansion), the amplitudes of atomic thermal vibrations (reflected in the Debye–Waller factor) and the colour centres are some examples of microproperties. In contrast, macroproperties are studied through measurements on material in bulk. Elastic properties, hardness, dielectric properties and melting temperature are examples of macro-properties.

The approach is to discuss in detail the physics of some select properties. Theoretical as well as experimental aspects are kept in view. The beginnings of studies of these properties can be traced to the earlier part of the last century. Due to the basic nature of these properties, there has been continuing research interest and constant refinement of the experimental methods. New levels of accuracy in measurement have made it possible to observe second-order changes like the effects of temperature, pressure, magnetic field, radiation, impurities and other defects; thin film and particle size effects have also been studied. Apart from bringing out the fundamental aspects, the book also provides considerable space for a discussion of current trends in research in the form of a comprehensive 'overview'. Typically, in each chapter, the earliest reference pertains to the period 1910–1930 and the latest to the period 1995–2005. The behaviour of a variety of materials like metals, alloys, ionic crystals, semiconductors, mixed valence compounds, optoelectronic materials and biomaterials is discussed vis-à-vis these properties.

Chapter 1 deals with the lattice constant which is a fundamental attribute of a crystal lattice. Various methods of accurate determination of lattice constants are discussed. The accuracy in lattice constant measurement has now reached almost the limit as it is of the same order as the accuracy in wavelength measurements. Effects of irradiation, impurities, deuteration of hydrogen-containing compounds and particle size are discussed. Chapter 2 is on thermal expansion of solids. A variety of experimental methods are

described including some novel techniques which use holography and gamma ray absorption. The intimate relation between thermal expansion and anharmonicity of lattice vibrations is brought out and the important role of thermal expansion in throwing light on thermally generated defects is pointed out. Chapter 3 is devoted to the Debye–Waller factor which is related to the amplitudes of atomic thermal vibrations. Originally introduced as a correction for X-ray diffraction intensities, it has emerged as a powerful solid-state probe. It is related to the lattice dynamical models, the interatomic bond strength, the lattice strain and surface forces. The hardness of crystals forms the subject of Chap. 4. Starting with microhardness methods, recent techniques of ultra and nanohardness are discussed. A variety of aspects are included like temperature and pressure variation and effects of magnetic field, irradiation and chemical bonding. An interesting new observation is the study of phase transitions through micro-Raman spectroscopy of indentations obviating the use of a diamond anvil. Chapter 5 on the dielectric behaviour of materials starts with the basics of dielectrics. Experimental techniques for different frequency ranges are considered. It is shown that dielectric properties throw much light on such diverse aspects as anharmonicity, spectroscopic phenomena, defects and chemical bonding. Various conduction mechanisms are discussed including polaron conduction. The dielectric behaviour of organic compounds and biomaterials is considered along with inorganic compounds.

To complement the experimental approach, the theoretical approach to solid-state properties is developed in Chap. 6. The evaluation of thermal parameters like the Debye temperature and Gruneisen constants and also mechanical properties like elastic constants is discussed. A new method for the evaluation of the Raman mode Gruneisen parameter of fluorite type crystals from dielectric properties is included. A comprehensive treatment of mixed crystal physics is given in Chap. 7. The properties of mixed crystals are intermediate between those of the parent compounds. This creates the possibility of controlling the properties by controlling the mixed crystal composition. Several properties like hardness, dielectric constant, formation energy of defects, effective ionic charge, colour centre wavelengths, melting points, Debye–Waller factors and transition temperatures are discussed with reference to their composition dependence. Chapter 8 on the elastic properties of solids is mainly focused on the serious problem of discrepancies in elastic properties and some possible checks.

The choice of the properties included in this book was, to some extent, influenced by the research interests of the authors. Considerable amount of work was generated through the research programmes undertaken by the authors over several decades. Instead of including the results of our work in the 'overview', they are presented as a separate section entitled 'Some of our results' in each chapter. We had the privilege of having Prof. K.A. Gschneidner (Jr.) and Dr. B.J. Beaudry (Iowa State University), Prof. B.S. Shah (Saurashtra University) and Dr. B.R. Rao (Indian Institute of Chemical Technology) as collaborators. A large number of Ph.D. and M.Phil. students were also

associated with our work. While reference has been made to them at appropriate places as co-authors, we would like to place on record our appreciation of their role in our research programmes.

We are thankful to Dr. K.S. Rajam and Dr. H.C. Barshilia (National Aerospace Laboratory, Bangalore) for sharing information on nanoindentation. Thanks are also due to Prof. K.G. Nickel (University of Tubingen) for providing material on micro-Raman spectroscopy of indentations. The chapter; Elastic Properties of Solids – 'A Critical Analysis' is a modified version of a recent Review Article: 'Consistency Checks on Elastic Properties of Solids' published by two of the authors (DBS, KGS) in the Journal of Materials Science. Grateful thanks are offered to colleagues at Kluwer Publishers and their successors, Springer, for kind permission to use substantial material from the review.

We would like to thank Prof. K.G. Bansigir (Jiwaji, University), Dr. Ch. V. Purushotham Reddy (Chaitanya Educational Institutes) and Mr. Vinod Kumar (South Asian Publishers) for much interest. Thanks are offered to colleagues at the Kakatiya University for their support and cooperation.

Finally, we are grateful to Dr. C. Ascheron of Springer-Verlag for timely suggestions and valuable advice during the various stages of the preparation of this book. The prompt response and patient guidance received from colleagues at the Hiedelberg office of Springer and at SPi, India are acknowledged.

Warangal, India
June 2006

Dinker Sirdeshmukh
Lalitha Sirdeshmukh
K.G. Subhadra

Acknowledgements

The following publishers are thanked for permission to reproduce illustrations and material from their publications:

1. American Institute of Physics
2. American Physical Society
3. Current Science Association
4. Elsevier Ltd.
5. Indian Academy of Sciences
6. Institute of Physics (UK)
7. International Union of Crystallography
8. Kluwer Publishers
9. Physical Society of Japan
10. Springer-Verlag
11. Wiley - VCH

Contents

1

Lattice Constant – A Solid State Probe

1.1 Introduction

The lattice constants are basic crystallographic parameters as they represent the dimensions of the unit cell. The number of lattice constants varies from 1 to 6 as we pass from the most symmetric (cubic) to the least symmetric (triclinic) crystal class. From the lattice constants, other crystal parameters and properties like molar volume, density and ionic radii can be estimated. The variations in lattice constants with temperature and pressure yield values of the thermal expansion coefficient and compressibility, respectively. The effects of thermally generated defects, doping and radiation induced defects can be followed through small, but significant, changes in the lattice constants. When determined with accuracy, the lattice constant provides rich information about the crystal and is a powerful solid state probe.

1.2 Experimental Methods

1.2.1 Principle

The determination of lattice constant is based on Bragg's law of X-ray diffraction illustrated in Fig. 1.1 and stated in (1.1).

$$n\lambda = 2d \sin\theta, \tag{1.1}$$

where, λ is the wavelength, d the interplanar spacing and θ the Bragg angle and n is the diffraction order parameter. A set of indices h, k, l, (called the Miller indices) is associated with each plane. Thus, (1.1) can be rewritten as

$$\sin^2\theta = \lambda^2/4d_{hkl}^2. \tag{1.2}$$

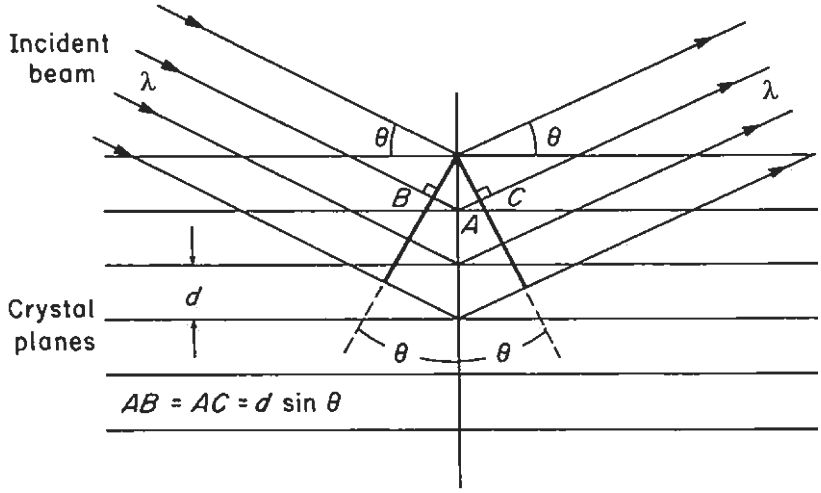

Fig. 1.1. Bragg's law

Expressing d_{hkl} in terms of the lattice constant 'a' and the Miller indices h, k, l, (1.2) takes the form

$$\sin^2\theta = (\lambda^2/4a^2)(h^2 + k^2 + l^2) \tag{1.3}$$

for a cubic crystal. The order parameter n is included in the Miller indices.

There are similar but more complicated equations for crystals of lower symmetry. Thus, in principle, the lattice constant can be determined with an experimental set-up that permits recording of X-ray diffraction reflections and the measurement of the associated Bragg angles.

1.2.2 Experimental Techniques

Several techniques are in use for recording X-ray diffraction patterns. For lattice constant determination, generally, powder methods are preferred. A comprehensive discussion of these methods is available in literature [1.1–1.4]. Some of the methods are discussed here.

The Debye–Scherrer Camera (DSC)

The geometry of this camera is shown in Fig. 1.2. Monochromatic X-rays enter through the collimator and fall on a needle-like powder specimen. The X-rays are diffracted both in the front and in the backward direction by different lattice planes. In the figure, lines with single arrow indicate incident and undiffracted rays and those with double arrows indicate diffracted rays. The undiffracted rays are absorbed in the exit port. The photographic film stays pressed against the inner surface of the cylindrical camera of radius R.

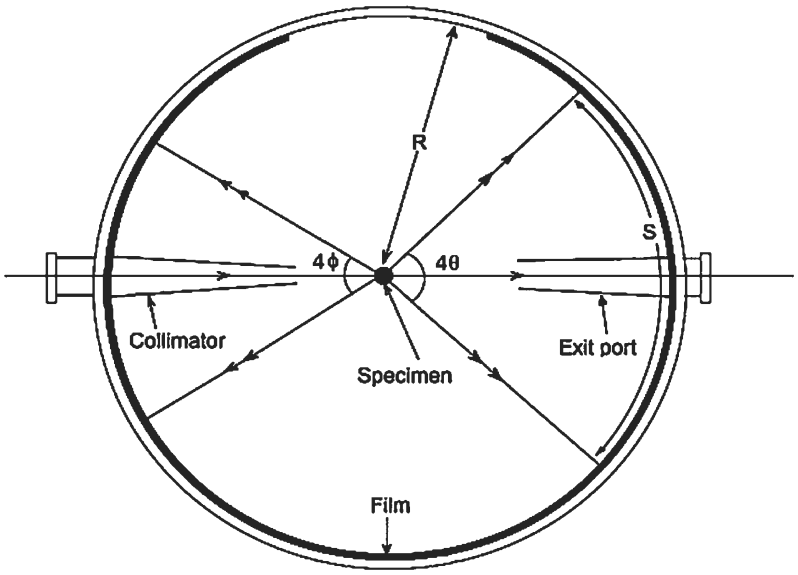

Fig. 1.2. Geometry of the Debye–Scherrer camera

Fig. 1.3. Debye–Scherrer photograph of Al

A typical photograph taken with this camera is shown in Fig. 1.3. Denoting the diameter of a Bragg reflection by S, the Bragg angle is given by

$$\theta = (S/4R)(180/\pi)^\circ \tag{1.4}$$

for forward reflection and

$$\theta = (\pi/2) - \phi = [(\pi/2) - (S/4R)]\ (180/\pi)^\circ \tag{1.5}$$

for back reflection. Generally, the diameter of a DSC is 11.46 cm. The mounting of the film is called 'Straumanis mounting'. It facilitates recording of the ring systems in front reflection ($\theta < 90^\circ$) as well as back reflection ($\theta > 90^\circ$). Further, by measuring the distance between the centers of the two punched holes, the effective radius of the camera can be determined.

Unicam-Type Camera (UC)

A critical examination of the commercially available Unicam camera revealed that it has the following drawbacks:

1. It employs the Bradley–Jay mounting with two film strips. The center of the ring system is not included on either strip making the use of knife edges unavoidable.
2. The specimen centering device is not convenient to operate and is not easily accessible. In the original design, the specimen is suspended from above.
3. The platinum-wound heater is excellent but its spherical design makes any repair impossible and replacement is too expensive.

A Unicam-type cylindrical camera with 19 cm diameter has been designed and fabricated [1.5]. While the design is essentially similar to the Unicam model, some of the drawbacks in the original design have been overcome. As this camera was indigenously fabricated in the authors' laboratory, the design and operation are discussed in detail.

The principle of the cylindrical camera is shown in Fig. 1.4. This is similar to the Debye–Scherrer camera (Fig. 1.2) but with a difference in film mounting which will be discussed later. The film forms a cylinder at the axis of which the powder sample in the form of a thin cylindrical rod is located; for thoroughly random orientation of the crystallites, the specimen is rotated about its own axis. The incident rays enter through a collimator and the direct ray is stopped by a beam stopper. In a back reflection camera, the diffracted rays travel backward (with respect to the incident beam) along a cone of angle 4ϕ where $\phi = (\pi/2) - \theta$.

The essential parts of the camera are shown in Fig. 1.5. These are: the main base (A), the base plate (B), the specimen holder (C), the central brass

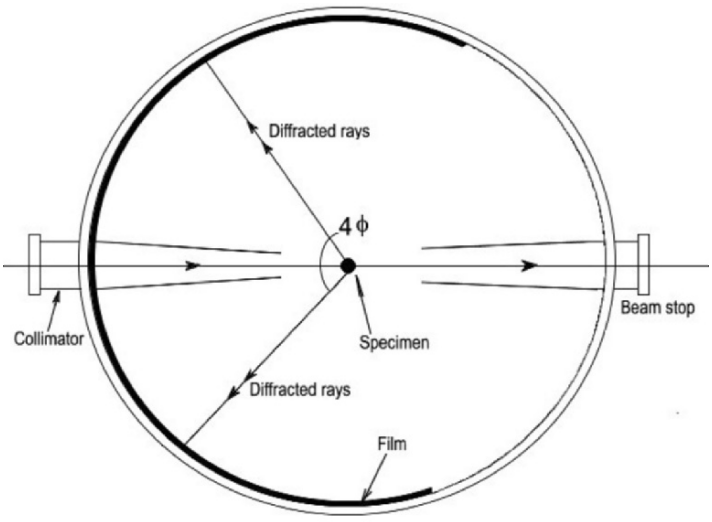

Fig. 1.4. The principle of the Unicam-type cylindrical camera

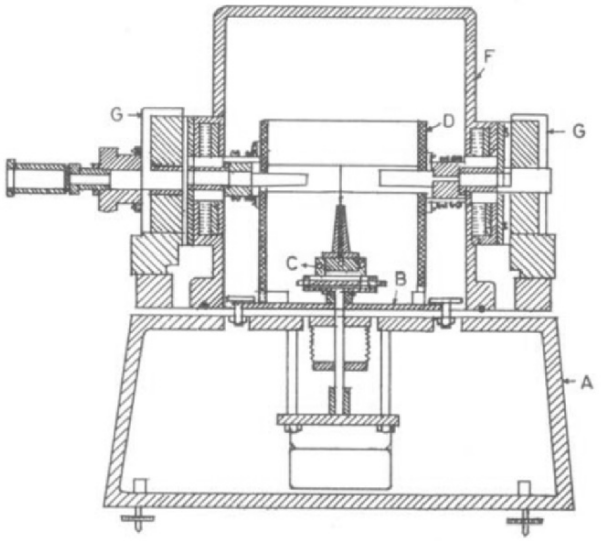

Fig. 1.5. Essential parts of the cylindrical camera

cylinder (D), the heater (E) (not shown in the figure), the evacuation chamber (F) and the film cassette (G).

As mentioned earlier, the specimen holder is different from that in the Unicam camera. Its design is shown in Fig. 1.6. The centering of the specimen is accomplished by the device shown in Fig. 1.6a (top view) and Fig. 1.6b (cross-section). The specimen is mounted in a cavity drilled in the top portion of a thin brass rod (A) which has a circular base (B). The base is rigidly fixed over a small horizontal table (C) which is fixed in a slot by means of a screw (D) with stoppers at the ends. To obtain transverse motion of table (C) another similar table (E) is fixed below (C). Table (E) is fixed with screw (F). The two screws (D) and (F) are at right angles to each other and enable the specimen to be moved linearly. A brass bush is fixed at the bottom of the lower table (E). The entire arrangement is mounted on a shaft with a provision to lock it on to the shaft or to release it. The sample filled in a thin capillary tube is fixed in the cavity of the brass rod (A) using dental cement. Centering of the specimen is checked by viewing it through a microscope fixed to the main base. The sample holder is released from the shaft and rotated to bring screw (D) to the right of the viewer. If the sample does not coincide with the vertical cross-wire in the microscope, screw (D) is manipulated suitably. The sample holder is then rotated through a right angle such that screw (F) is on the right and the specimen is again centred using screw (F). This process is repeated until no displacement is observed from the axis of rotation. The specimen holder is now locked on to the shaft. The other end of the shaft connects with

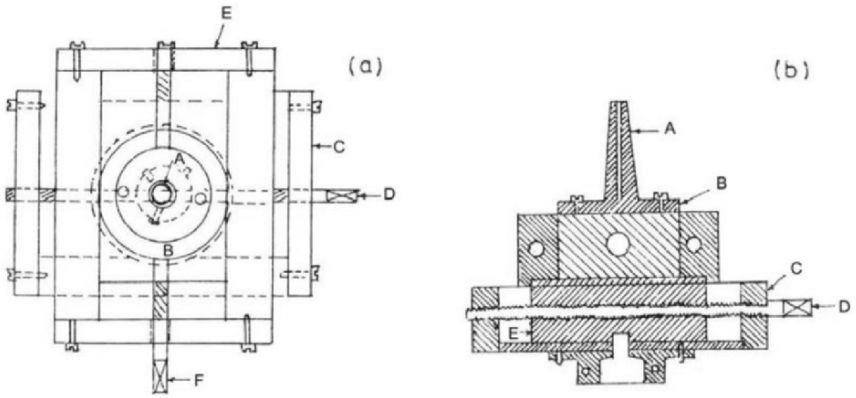

Fig. 1.6. (a) Top view, (b) cross-section of the specimen holder for the camera in Fig. 1.5

the spindle of a 1 rpm motor. When the film cassette is in position, the sample may be observed by its shadow on the fluorescent screen of the beam stop.

For determination of lattice constants at high temperature, a heating arrangement is necessary. The chief requirements of high temperature operation are the temperature stability over a period of 6–10 h and the measurement of specimen temperature. A suitable design is shown in Fig. 1.7. A hollow tube (A) of length 6 cm and diameter 1.5 cm with a slot (B) and a hole (C) at the center is brazed at its top to a circular disc (D). The slot is of width 10 mm extending around the tube over an angle of 220° and is at right angles to the axis of the tube. The hole permits the incident X-ray beam to strike the specimen and the slot allows the diffracted beam to pass out to the film. A refractory hollow tube (E) of thickness 1 cm with a similar slot and hole is compounded with the brass tube. The refractory tube snugly fits over the brass tube. The refractory tube has linear holes all round through which a coiled super-kanthal wire (G) is passed. A thin circular asbestos plate (H) with a central hole of diameter 2 cm is fixed on the lower side of the disc (D) to prevent heat losses due to conduction. The lead wires of the coils are brought out to the terminals through a small two-holed ceramic tube (I) fixed in a hole drilled in the brass disc. There is a hole at the center of the disc through which a brass bush (J) of length 2.7 cm is press-fitted into the brass tube. Two two-holed ceramic tubes (K, L) are rigidly fixed vertically in the holes drilled at the bottom of the bush. The lower ends of the ceramic tubes just enter into the gap provided for the passage of diffracted X-rays. Chromel–alumel thermocouple wires are passed through the ceramic tubes such that their junctions (M, N) lie very close to the specimen on either side of the portion of the sample exposed to X-rays.

The entire assembly is inserted in the central brass cylinder. A circular groove (F) is engraved in the disc (D) on the side facing the base of the

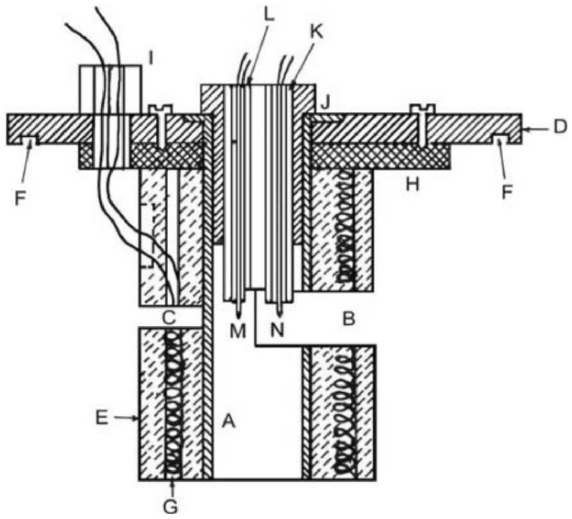

Fig. 1.7. Heating unit for the camera in Fig. 1.5

camera and fits on the top of the central brass cylinder. The disc can be rotated horizontally about the axis of rotation of the sample holder and can be fixed such that the incident X-ray beam after passing through the hole in the heater strikes the sample and diffracted X-rays reach the film arranged to receive backward reflection. The heater wire and thermocouple wires outside the heater are passed through ceramic beads. The free ends of the heater and thermocouple wires are connected to the terminals on the base plate of the camera. The thermocouples are connected to two separate millivoltmeters. The heater is fed from an AC supply through a stabilizer and a variac. A temperature of about 800°C can be attained within 20 min. The temperature stability is obtained by adjusting the output of the variac to give a constant voltage. The temperature distribution in the heater was investigated by positioning the thermocouple along the exposed length of the specimen. It was observed that the temperature remains fairly steady along the length of the specimen exposed to X-rays. The temperature recorded by the two thermocouples always agreed within 0.5°C. The constancy of temperature with time is excellent once the equilibrium is reached. The fluctuation in temperature during exposure was $< \pm 1$°C up to 400°C and $< \pm 2$°C at higher temperatures. The heater is so designed that it can be lifted in and out of the camera as a single unit during the sample mounting and alignment procedure. Also if the heater element is burnt out it can be replaced easily.

Unlike the original Unicam camera which employs Bradley–Jay film mounting, Van Arkel type of mounting is employed in this camera. With this mounting, both sides of the ring system are recorded and the ring diameters of back reflection lines can be measured without the need for knife-edge or any other calibration. A photograph of the camera in the assembled form is

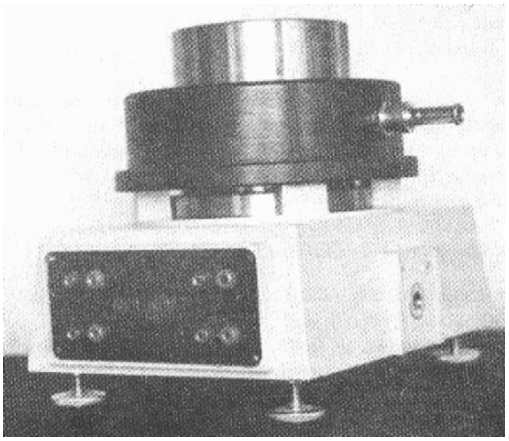

Fig. 1.8. Photograph of the cylindrical camera

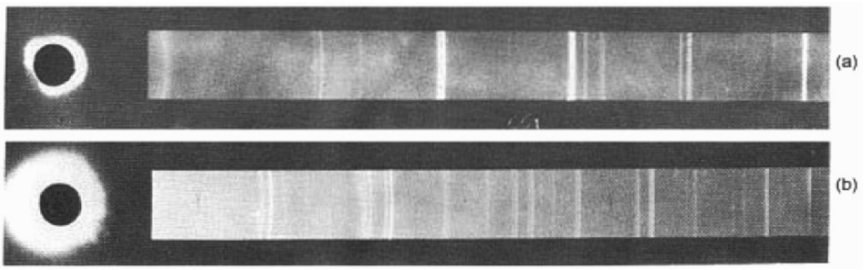

Fig. 1.9. Diffraction pattern for (a) MgO and (b) PbF_2 taken with the cylindrical camera

shown in Fig. 1.8. As will be discussed later, the error function suitable for this camera is $f(\theta) = (1/2)\,[(\cos^2\theta/\sin\theta) + (\cos^2\theta/\theta)]$.

As examples, the diffraction patterns of MgO and PbF_2 obtained with this camera are shown in Fig. 1.9. The extrapolation plots are shown in Fig. 1.10.

Symmetric Focusing Camera (SFC)

The geometry of a symmetric focusing camera is shown in Fig. 1.11. The basic principle of the design of a symmetric focusing camera is that if a divergent beam of X-rays falls on a sample spread over a cylindrical surface, the diffracted beam is focused provided the slit, the sample and the film lie on a circle called the focusing circle. When these conditions are satisfied, the reflections are sharp and intense. Further, since the effective film-to-specimen distance is large, compared to that in a Debye–Scherrer camera of the same radius, the resolution is larger.

A camera based on this principle designed by Sirdeshmukh and Deshpande [1.6] is described. The camera is 15 cm in diameter. From a carefully cut

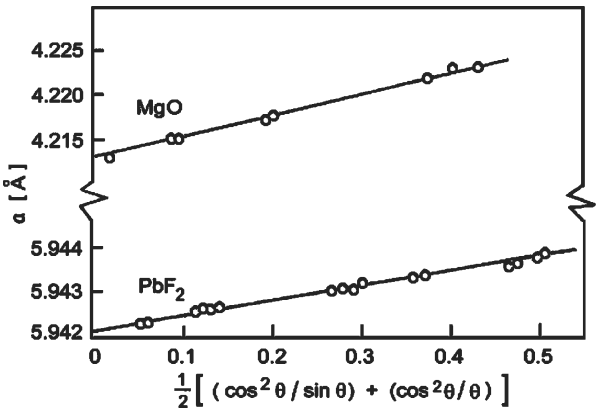

Fig. 1.10. Extrapolation plots for (a) MgO and (b) PbF_2

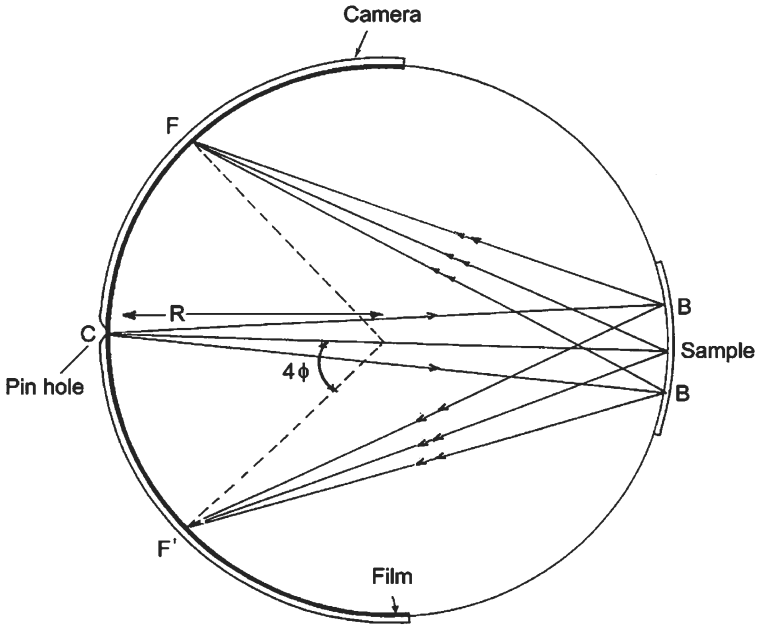

Fig. 1.11. Geometry of a symmetric focusing camera

cylinder, a minor segment is cut away. The major segment is the film-holder. It can record reflections with Bragg angles in the range of 65° onwards. The main parts of the camera are shown in Fig. 1.12. It has at its base a tripod (A) with leveling screws (B). The tripod carries a horizontal bench (C) which can rotate about a vertical axis. It can be locked onto the tripod by means of the screw (D). The horizontal bench carries an upright (E) which consists of a fixed piece and a sliding piece. The slider can be moved up and down

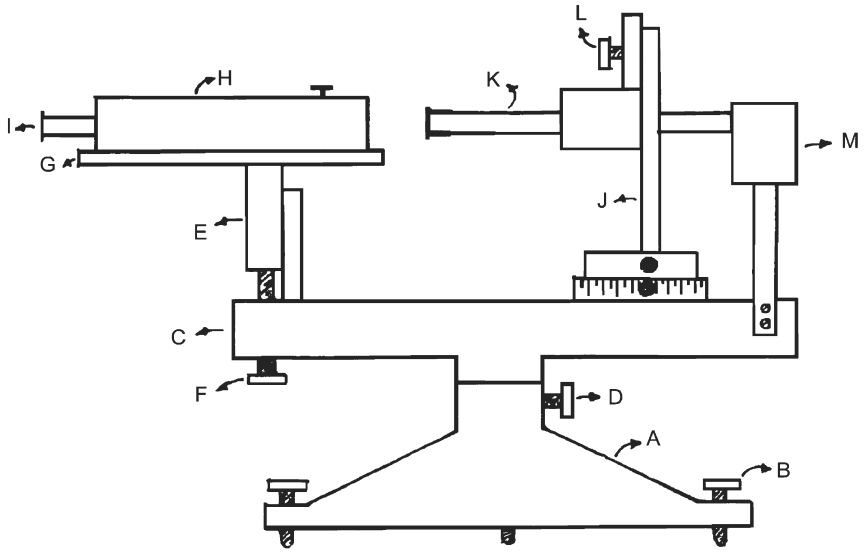

Fig. 1.12. Main parts of the symmetric focusing camera

Fig. 1.13. Diffraction pattern of aluminium using the symmetric focusing camera

by the micrometer screw (F). At the top of the sliding piece is a platform (G) which carries the film holding assembly (H) along with the collimator (I). The upright (J) is mounted over the horizontal bench. The upright can be displaced towards or away from the film-holder. There is also provision for lateral displacement of the upright. At its top the upright carries the sample holding tube (K) which can be displaced in the vertical direction by means of the screw (L). The tube is coupled to a motor (M) through an eccentric cam.

For convenience a flat sample is used instead of a sample with a cylindrical surface. The systematic errors in this camera have been analysed and it was found that the function $\phi \tan \phi$ is a suitable error function. Here $\phi = (\pi/2)–\theta$. A diffraction photograph of Al is shown in Fig. 1.13 and the extrapolation plot for Al is shown in Fig. 1.14. The extrapolated value of 4.0499(2) Å agrees well with the value 4.0499(1) Å obtained by Wilson [1.7].

For lattice constant measurement at higher temperatures, a tubular heater is introduced such that the sample surface is at the central region of the heater. The temperature is measured with a copper–constantan thermocouple welded at the back of the sample holder.

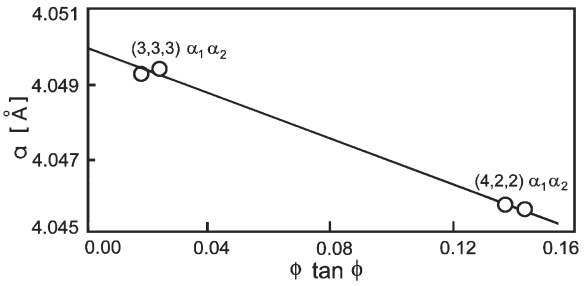

Fig. 1.14. Extrapolation plot for Al

Flat Film Camera (FFC)

The geometry of the flat film camera is shown in Fig. 1.15. As the name indicates, a flat film is employed. For accurate determination of lattice constants, the back-reflection geometry is used. Because of the limitation of size of the film, only a few reflections are recorded (Fig. 1.16). If S is the diameter of a ring and D the film-to-specimen distance, the angle θ is given by

$$\theta = (\pi/2) - \phi = [(\pi/2) - (1/2)\tan^{-1}(S/2D)]\,[180/\pi]^\circ. \qquad (1.6)$$

X-Ray Powder Diffractometer

The X-ray diffractometer is a versatile technique which facilitates at once the measurement of the Bragg angle of a reflection, its intensity and its profile.

The detection of the diffracted beam is done with a GM counter (almost obsolete now) or a proportional counter or a scintillation counter. The electronic circuitry for stability and detection is quite involved. Detailed discussion of these aspects is given in the texts mentioned at the beginning of this section. The specimen preparation is to be done with care (see Chap. 3). The geometry of the system shown in Fig. 1.17 and described later follows the treatment by Peiser et al. [1.1].

The point of divergence A is the line focus of the X-ray tube. BOB′ is the trace of the specimen. The detector C is carried on the arm pivoted at O; OA and OC are equal. The detector and the sample rotate maintaining a θ–2θ relationship so that ON, the normal to BOB′ always bisects $\angle$AOC. AOC is the focusing circle. The detector moves along the circle described about O. The focusing circle AOC (which has no physical reality) changes continuously as the sample and detector traverse. This is known as the Bragg–Brentano focusing system.

While the instrument uses a divergent beam, it is also necessary to limit the divergence. This is done with the help of special devices known as Soller slits. As the detector occupies some length, its movement restricts the angular region that can be explored – generally up to $\theta = 60^\circ$. For accuracy in lattice

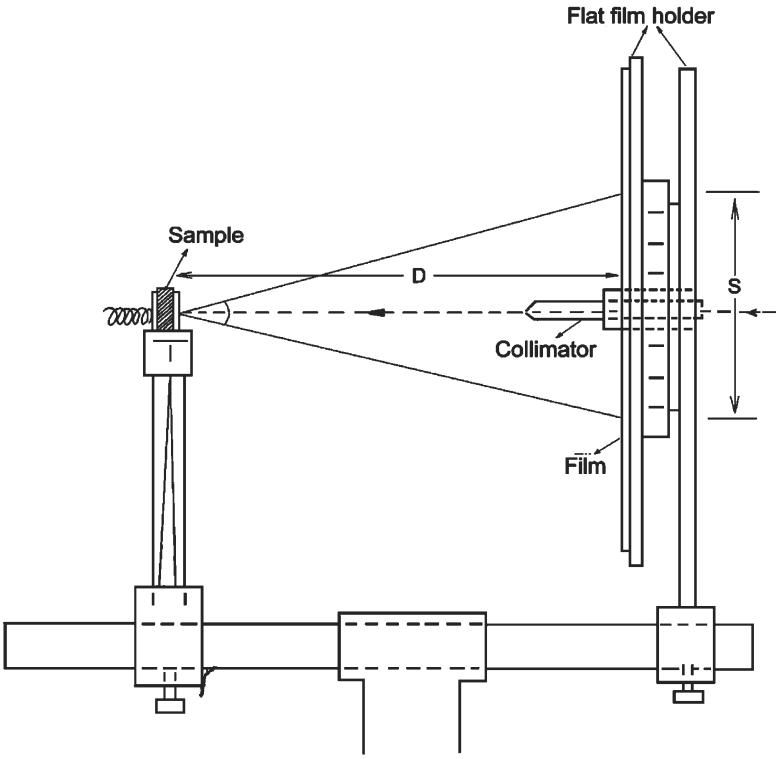

Fig. 1.15. Geometry of the flat film camera

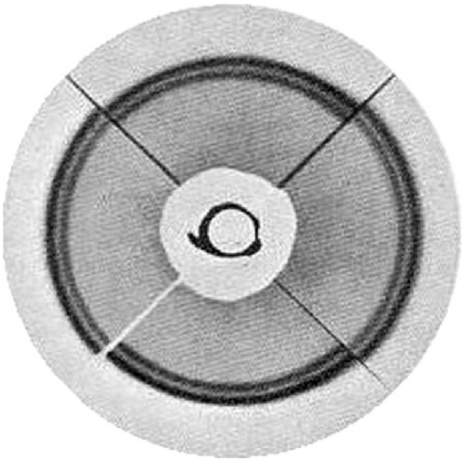

Fig. 1.16. Powder photograph of two silver gold alloys using a flat film camera

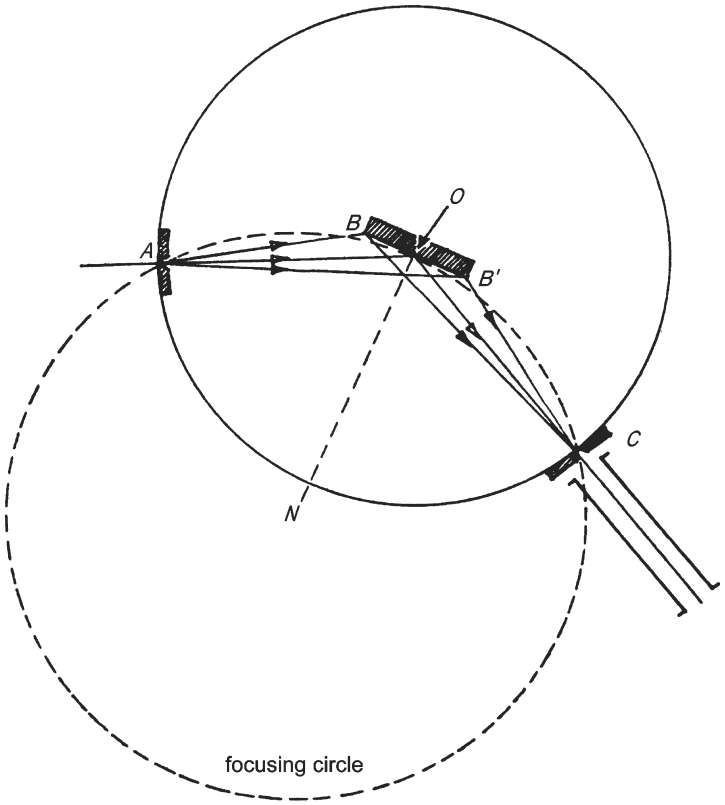

Fig. 1.17. Geometry of the X-ray powder diffractometer

constant determination, higher angles are preferred (see Sect. 1.2.3). However, because of the distances involved, the stringent geometry and the efficient detection, the XRD has a high resolution even at low angles. A typical XRD pattern is shown in Fig. 1.18.

Most of the commercial models of diffractometers are based on the principles discussed in the preceding paragraphs. However, in Bond's [1.8] diffractometer, a single crystal is employed and two wide-aperture detectors are placed in the symmetric back-reflection configuration (Fig. 1.19). The crystal is turned so that a reflection from the crystal is recorded by the two detectors in succession. A high precision is obtained by this method.

1.2.3 Strategies for Accuracy

Errors occur in the determination of lattice constants. These errors are of two types: systematic and random. Differentiation of the Bragg equation leads to

$$(\Delta d/d) = -(\cot\theta)\Delta\theta. \tag{1.7}$$

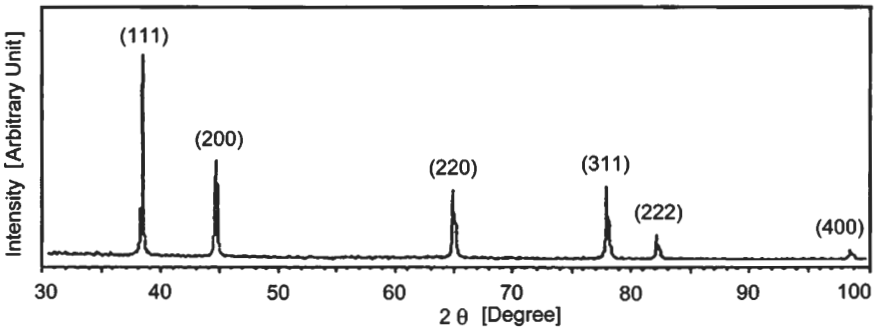

Fig. 1.18. Typical X-ray diffractogram of a powder sample (Ag)

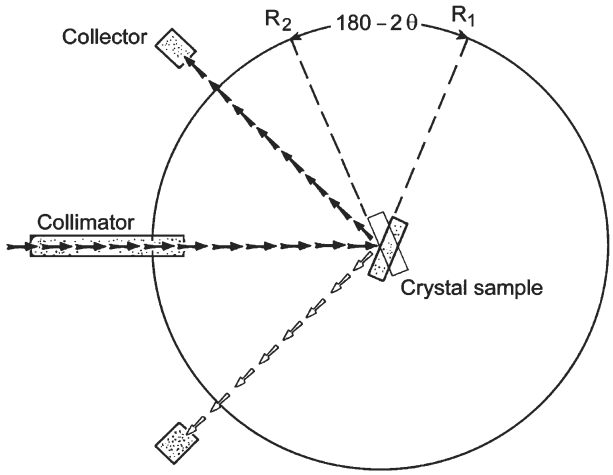

Fig. 1.19. Geometry of Bond's (single crystal) diffractometer

Thus an error $\Delta\theta$ in the measurement of the angle results in a large error $(\Delta d/d)$ at low angles and a smaller error at high angles. In fact $(\Delta d/d) \to 0$ as $\theta \to 90°$. Hence, the first strategy for accurate determination is to use high angle reflections, generally $\theta > 60°$.

But the effect of errors still remains to be attended. Systematic errors arise due to errors in geometrical parameters or physical effects. For instance, in a cylindrical camera, errors may arise due to the following causes:

1. Error in camera radius
2. Displacement of sample from camera center
3. Absorption of beam by sample
4. Divergence of beam

Table 1.1. Error functions for different techniques

	Technique	f(θ)	f(θ) at high θ
i	Cylindrical (DSC and UC) camera	$\frac{1}{2}\left[\frac{\cos^2\theta}{\theta}+\frac{\cos^2\theta}{\sin\theta}\right]$	$\cos^2\theta$
ii	Flat film camera (back reflection)	$\cos 2\phi - \cos^2 2\phi$	$\cos^2\theta$
iii	Symmetric focusing camera	$\phi\ \tan\phi$	$\cos^2\theta$
iv	Diffractometer	$\cos\theta\cot\theta$	$\cos^2\theta$

The errors have been worked out and it has been shown that $(\Delta d/d)$ is a function of the Bragg angle. Thus,

$$(\Delta d/d) = f(\theta), \tag{1.8}$$

where $f(\theta)$ is the error function. Error functions for various techniques are given in Table 1.1. It may be seen from the table that in each case $f(\theta) \to 0$ as $\theta \to 90^\circ$. For a cubic crystal

$$\Delta d/d = \Delta a/a. \tag{1.9}$$

From (1.8) and (1.9), it follows that:

$$\Delta a = a_{\text{obs}} - a_{\text{true}} = a_{\text{true}}\ f(\theta). \tag{1.10}$$

Hence, a plot of a_{obs} obtained from each reflection against the corresponding $f(\theta)$ will be a straight line. When this line is extrapolated to $\theta = 90^\circ$ the intercept gives a_{true}.

Random errors are minimized, first, by measuring θ repeatedly and taking the mean and, second, by drawing the extrapolation plot by least square analysis. Instead of a graphical extrapolation, Cohen [1.9] suggested error elimination by a least square processing of the data starting with the $\sin^2\theta$ values.

1.2.4 Present Level of Accuracy

A summary of the accuracy in lattice constant measurement possible with different methods is given in Table 1.2. It can be seen that an accuracy of one part in (1–5) $\times 10^4$ can be achieved with routine methods while a higher accuracy of one part in (1–2) $\times 10^5$ is possible with special methods. This is just an order less than the accuracy in X-ray wavelengths [one part in (5–10) $\times 10^5$]. Results of some studies where lattice constants have been measured with very high accuracy are given in Table 1.3.

1.3 An Overview

There is an enormous amount of information on the lattice constants of materials. This information is scattered in a vast number of papers published

Table 1.2. Accuracy of lattice parameter determination by various methods

Method	Accuracy in a
	1 part in
Rotating crystal camera	$< 10{,}000$
Weissenberg camera	$< 10{,}000$
Debye–Scherrer camera	15,000
Diffractometer (asymmetric)	15,000
Unicam camera	50,000
Focusing camera	50,000
Kossel line method	100,000
Bond's method	200,000
Uncertainty (in λ)	500,000

Table 1.3. Accurate values of lattice constants (a) of some crystals; method and accuracy given wherever mentioned in source

Crystal	Method	Temperature [°C]	a [Å]	Ref.
Al		25	4.04958	[1.10]
Au		25	4.07825	[1.10]
Cu		18	3.61496	[1.10]
NaCl		26	5.64056	[1.10]
NaBr		26	5.97324	[1.10]
KCl		25	6.29294	[1.10]
KI		25	7.06555	[1.10]
Diamond	FFC	25	3.56696(7)	[1.11]
W	DSC	25	3.16491(5)	[1.13]
Ge	Kossel	25	5.657736(8)	[1.14]
GaAs	Bond	25	5.653663(5)	[1.14]

in various journals. Among them, mention may be made of Acta Crystallographica, Proceedings of the Physical Society (London), Journal of the Physical Society of Japan, Journal of Applied Physics and Journal of Chemical Physics. Exhaustive compilations of data on lattice constants is available in [1.10, 1.15, 1.16]. In this section, some studies where the measurement of lattice constant has been used to probe various physical phenomena in solid state are discussed.

1.3.1 Characterisation of Semiconductor Materials

For semiconductor devices, material with highest purity and free from defects is required. The lattice parameter provides a useful control on device material. Silicon being the most commonly used semiconductor material, its lattice parameter has been determined with very high precision so much so that it is now used as a standard in X-ray diffraction instrumentation. Some results on the lattice parameter of silicon are given in Table 1.4. There is good internal consistency among the values of the lattice parameters obtained by various

Table 1.4. Lattice constant of silicon

Single crystal sample		Powder sample	
a [Å]	Ref.	a [Å]	Ref.
5.43108	[1.17]	5.43085	[1.12]
5.43106	[1.18]	5.43090	[1.21]
5.43107	[1.19]	5.43089	[1.22]
5.43107	[1.20]	5.43092	[1.20]

workers using single crystal samples. Similarly, there is agreement among the results obtained using powder samples But between the two sets of results (single crystal and powder), there is a consistent difference of 0.00015 Å, the value for the single crystal sample being larger. Parrish [1.12] suggested that this difference may be caused by the formation of a layer of SiO_2 formed in the process of grinding. A more plausible explanation is given by Hubbard et al. [1.20] in terms of crystal boundary effects.

Doping has significant effect on semiconductor behaviour. The addition of impurities alters the carrier concentration and hence the electrical behaviour. Tap et al. [1.23] and Gille and Schenk [1.24] studied the effect of doping PbTe with Bi and Tl ions on the lattice parameter. The addition of Bi ions reduces the lattice parameter. This is to be expected since the ionic radius of Bi^{3+} is smaller than that of Pb^{2+}. Although the radius of the Tl^{+} ions is larger than that of Pb^{2+}, the lattice parameter decreases on addition of Tl^{+} ions. This is explained on the basis of a difference in the binding between Tl and Te in relation to that between Pb and Te on the basis of complexes formed by Tl^{+} with the vacancies in PbTe.

1.3.2 Characterisation of Doped Crystals

Doping of crystals (addition of small but controlled quantities of impurities) has an effect on many physical properties of crystals. The effect is particularly prominent in optical, mechanical and electrical properties. Doping also has an effect on the lattice parameter and hence the lattice parameter can be used to characterize doped crystals.

Stott et al. [1.25] measured the lattice parameters of calcium fluoride doped with La, Tm and Y ions. The results are shown in Fig. 1.20. It is seen that the addition of rare earth ions results in an increase in the value of the lattice parameter. The per cent change in lattice constant for unit molar fraction of impurity has values 6, 6 and 13 for Y, Tm and La, respectively, and thus seems to depend on the radius of the rare earth ion. Another observation is that the value of the lattice parameter varies slightly depending on the section of the crystal boule from where the specimen is chosen. This indicates that the distribution of the impurity within the crystal is slightly inhomogeneous.

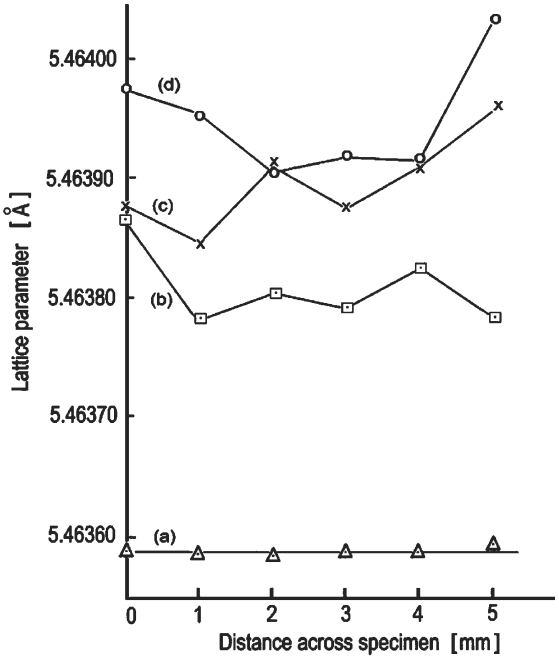

Fig. 1.20. Lattice parameters of: (**a**) undoped CaF_2; (**b**) CaF_2 containing 0.074 mol% TmF_3; (**c**) CaF_2 containing 0.088 mol% YF_3 and (**d**) CaF_2 containing 0.045 mol% LaF_3

1.3.3 Effect of Deuteration on Lattice Constants

The substitution of hydrogen by deuterium in hydrogen-containing substances is seen in lattice constant changes. Zimmerman [1.26] made measurements of lattice constant of crystals in the LiH_xD_{1-x} system. The lattice constants of LiH and LiD are 4.0831(4) and 4.0684(5) Å. The composition dependence of the partially substituted crystals was found to be linear.

Belouet et al. [1.27] studied the effect of deuteration on potassium dihydrogen phosphate (KDP) crystals. KDP is a tetragonal crystal. It can be seen from Fig. 1.21 that the 'a' parameter varies continuously with the deuteration parameter x. Further in the high x region, the measured values of 'a' show negative deviations from additivity. On the other hand, there is no systematic variation in the 'c' parameter due to deuteration.

1.3.4 Effect of Hydrogen on Lattice Parameters of Rare Earth Elements

The rare earth elements easily absorb hydrogen and this causes changes in the lattice parameter. A systematic study was made by Spedding and

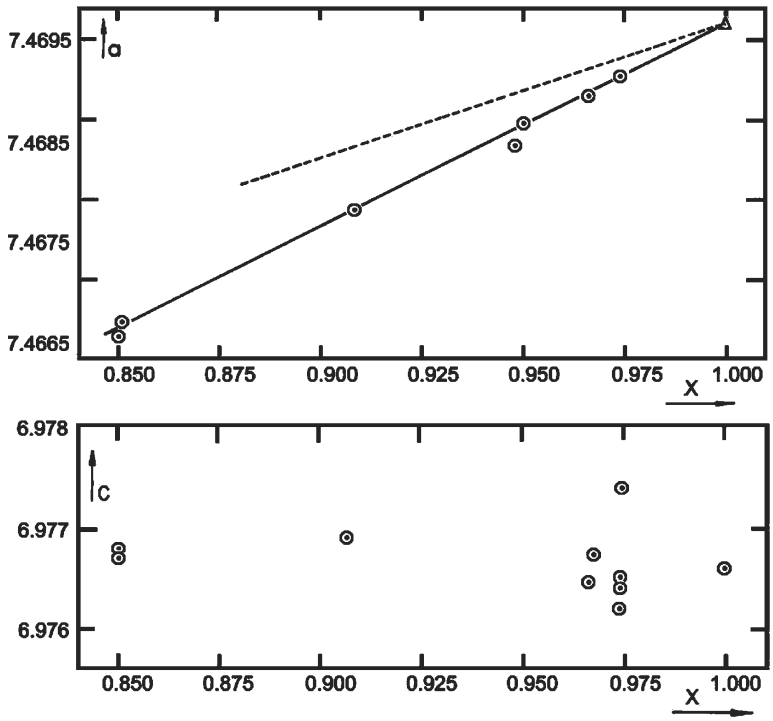

Fig. 1.21. Plot of lattice parameter a (Å) and lattice parameter c (Å) against deuteration parameter x of $KH_{2(1-x)}D_{2x}PO_4$ crystals. *Dashed line* represents additive variation of 'a'

Beaudry [1.28]. Very pure rare earth metal samples were heated in a hydrogen atmosphere until saturation and the lattice parameters were determined with the help of a Debye–Scherrer camera. The observed changes are shown in Table 1.5 and also in Fig. 1.22. It is seen that (i) the lattice parameters increase with hydrogen treatment, (ii) the increase in the 'c' parameter is more than that in the 'a' parameter and (iii) the increments in 'a' and 'c' vary from element to element.

1.3.5 Lattice Constants of Mixed Crystals

Mixed crystals are an important class of materials. Typical data on the composition variation of lattice parameters of the KI–RbI mixed crystal system taken from Van Den Bosch et al. [1.29] are shown in Fig. 1.23. The lattice parameters a_C of a mixed crystal system A_xB_{1-x} generally follow the equation:

$$a_C^n = xa_A^n + (1-x)a_B^n, \tag{1.11}$$

Table 1.5. Lattice parameters of the ABAB rare earth metals [1.28]

Rare earth metal	Lattice parameter		Increase in parameter due to hydrogen	
	a[Å]	c[Å]	a [Å]	c [Å]
Gadolinium	3.6336 ± 4	5.7810 ± 5	0.0003	0.0008
Terbium	3.6055 ± 4	5.6966 ± 6	0.0007	0.0001
Dysprosium	3.5915 ± 2	5.6501 ± 4	0.0013	0.0017
Holmium	3.5778 ± 2	5.6178 ± 3	0.0032	0.0052
Erbium	3.5592 ± 2	5.5850 ± 3	0.0052	0.0115
Thulium	3.5375 ± 4	5.5540 ± 2	0.0092	0.0216
Lutetium	3.5052 ± 4	5.5494 ± 5	0.0224	0.0598
Yttrium	3.6482 ± 2	5.7318 ± 6	0.0103	0.0383
Scandium	3.3088 ± 2	5.2680 ± 3	0.0371	0.0347

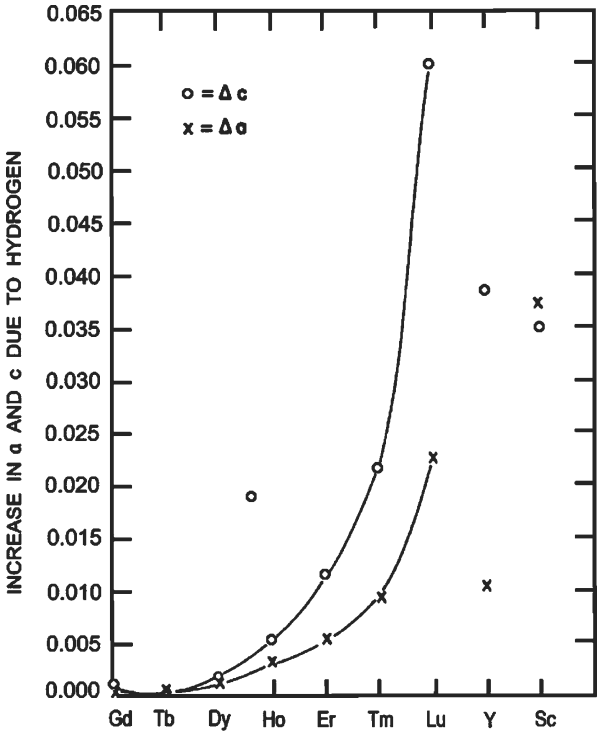

Fig. 1.22. Effect of hydrogen on the lattice parameters of rare earth metals

where a_A and a_B are the lattice parameters of the end members A and B, respectively, and x is the molar fraction of crystal A in the mixture. From the data on a number of systems, Sirdeshmukh and Srinivas [1.30] found that (1.11) with $n = 1$ provides the best description of the composition dependence

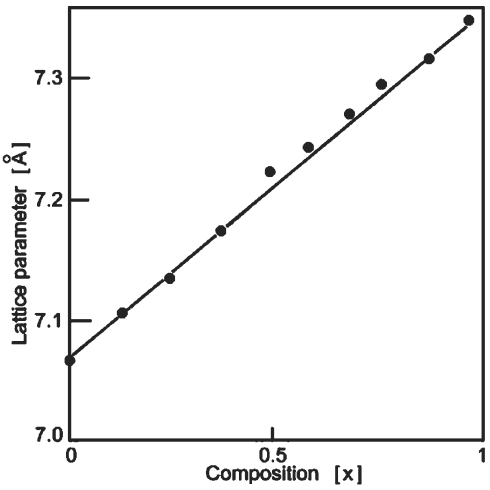

Fig. 1.23. Composition dependence of lattice parameters of $K_{1-x}Rb_xI$ mixed crystal

of lattice parameter in a mixed crystal system. Data on several mixed crystal systems will be discussed in Chap. 7.

Depending on the system, the composition of mixed crystals can be determined by potentiometric titration, polarography, atomic absorption spectroscopy or X-ray fluorescence. The lattice parameter can also be used as a means to estimate the composition. This method of characterisation has the advantage that using a small quantity of the material, lattice parameters can be measured with high accuracy.

1.3.6 Mixed Valence Effects in Lattice Constants

Mixed valence compounds have gained great prominence in recent years. The typical situation in these compounds is that the 5d bands of the rare earth ions are above the sharp 4f bands but the band gap is very narrow – often of the order of 0.5 eV. Under stimulation like pressure and temperature changes or by addition of other ions to the lattice, overlapping develops enabling the 4f electrons to participate in valence. Thus, several compounds belonging to this category show sudden changes in valence which, further, assumes a non-integral value.

In Fig. 1.24, the lattice parameter data obtained by Kaldis et al. [1.31] for the system $TmSe_xTe_{1-x}$ are shown. This system has the NaCl structure. The composition dependence of lattice parameter is very much different from that in Fig. 1.23 where it is linear. With the addition of Se, the valence of Tm suddenly changes from 2 to anywhere around 2.7. This results in the S-shaped curve. Here also, a number of parallel lines can be drawn to represent the

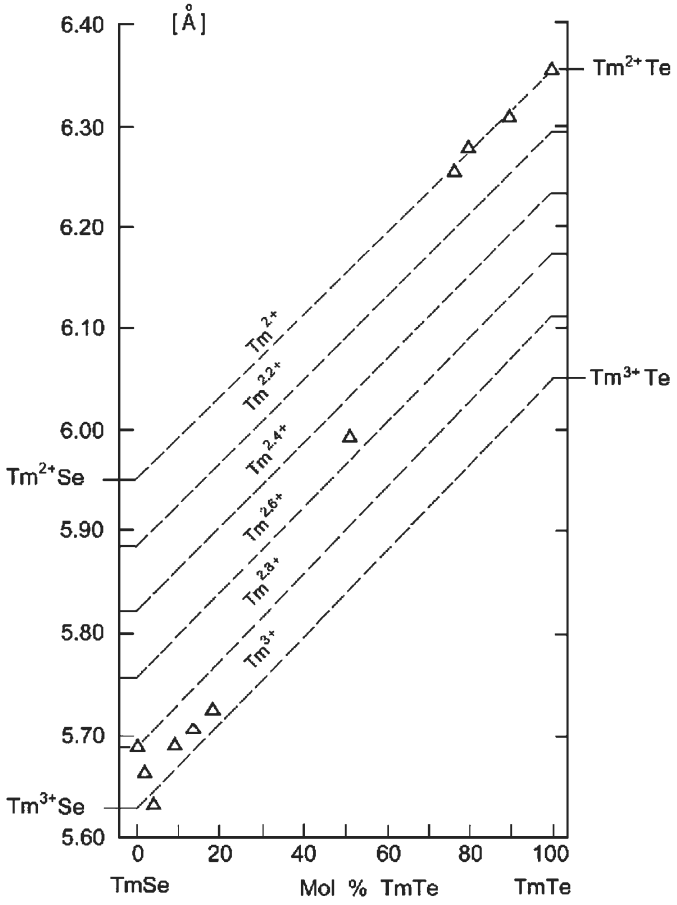

Fig. 1.24. Lattice parameters for the system $TmSe_xTe_{1-x}$

Vegard's law variation for a given value of valence. Thus the curve can be used to characterize the valence in these compounds.

Sampathkumaran and Vijayaraghavan [1.32] studied another interesting system – mixed crystals of $CeNi_2Si_2$ (which is a mixed valence crystal) and $CeCu_2Si_2$ (which is a heavy Fermion system). The lattice parameter variation with composition is shown in Fig. 1.25. Anomalous variation in the c parameter is observed at $x = 0.65$. At the same composition, anomalous variation is observed in magnetic susceptibility. It is suggested that the x-dependence of c may be useful in identifying heavy Fermion materials.

1.3.7 Temperature Variation of Lattice Constant

The temperature variation of lattice constant provides an important method for the determination of thermal expansion of crystals. The special advantage

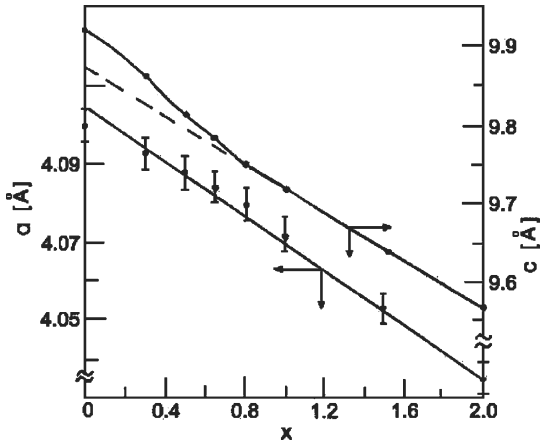

Fig. 1.25. Composition dependence of lattice parameters for the system $CeCu_{2-x}Ni_xSi_2$; dashed line indicates additive behaviour

of this method is that a very minute quantity of the material serves as sample. Further, in anisotropic crystals, the thermal expansion in several directions can be determined in a single experiment. Studies of temperature variation of lattice constants reveal many interesting phenomena like negative thermal expansion and phase transitions. Several studies of temperature variation of lattice parameters of crystals are cited in Chap. 2.

1.3.8 Pressure Variation of Lattice Parameters

By enclosing the sample in a pressure medium or in a diamond anvil press, the changes in lattice constant can be studied. From these changes, the linear compressibilities can be evaluated. A minute crystal or a small quantity of material in the powder form serves as sample. This method and results on several materials are quoted in Chap. 8.

1.3.9 Effect of Magnetic Field on Lattice Constant

There is very little work on this aspect. Kida et al. [1.33] studied the effect of magnetic field on the 'c' lattice constant of Dy which is antiferromagnetic with $T_N = 179\,K$ and ferrimagnetic with $T_C = 91\,K$. The study was carried out by making measurements on the (006) reflection from a single crystal using X-rays.

The variation of 'c' with magnetic field is shown in Fig. 1.26. There is a discontinuous change in 'c' in the experiments conducted at 130 and 150 K. This 'gap' in c-parameter vanishes at 170 K. The observations have been explained in terms of exchange integrals.

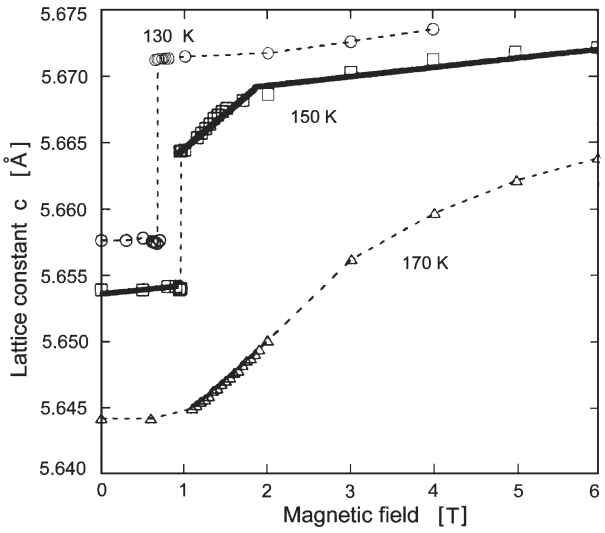

Fig. 1.26. Variation of lattice parameter c of Dy with magnetic field at different temperatures

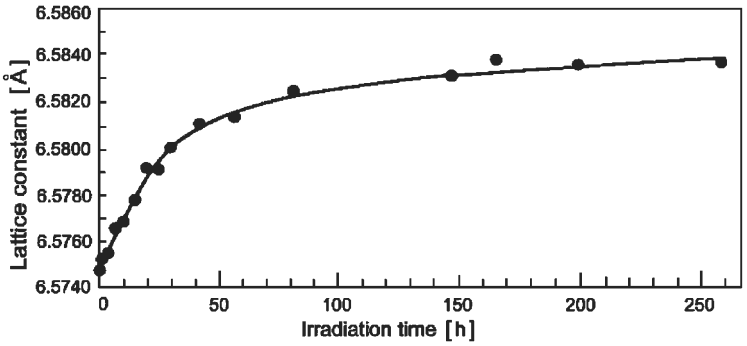

Fig. 1.27. Lattice parameter as a function of γ-irradiation time for $NaClO_3$

1.3.10 Radiation Damage

Irradiation of solids by high energy radiation affects several physical properties. Irradiation effects are seen in lattice parameter values also.

Stapien et al. [1.34] studied the damage in $NaClO_3$ crystals irradiated with γ-rays from a ^{60}Co source. The variation in the value of lattice parameter as a function of irradiation time is shown in Fig. 1.27. There is a fast increase in lattice parameter during the first 50 h of irradiation. Thereafter, the rate of increase slows down and the lattice parameter reaches a saturation value. There is considerable evidence to show that on irradiation the ClO_3 ion breaks

into a number of species including gaseous oxygen and ozone. The strains produced in the lattice by these radiolysis products result in the lattice parameter variations.

Zircon is a mineral of gem quality. It is a tetragonal crystal. It has been observed that zircon samples from different locations show a considerable range of physical properties. This applies to the lattice parameter values also. These variations cannot be explained in terms of differences in chemical composition. It is known that zircon samples invariably contain uranium and thorium as impurities. It has been suggested that the differences in lattice parameters are due to effects of irradiation by α-particles originating in the radioactive disintegration of uranium and thorium. That it is so can be seen from the plots of the lattice parameters a and c as a function of the α activity (Fig. 1.28). These results are taken from the work of Holland and Gottfried [1.35]. The plots are smooth curves. The observed variation could be due to a combination of causes like ionisation by the α particles and displacement of atoms by recoil nuclei.

The interesting result of this study of lattice parameters of zircon is that since lattice parameters are found to correlate with α-activity and since the latter correlates with the age of the mineral, it may be possible to use the lattice parameter as a measure of the age in zircon samples.

1.3.11 Effect of Particle Size on Lattice Constant

A smaller particle size shows two effects on X-ray (or electron) diffraction patterns. First, there is a broadening of the powder diffraction lines and, second, there is a measurable change in the lattice constant. A detailed electron diffraction investigation by Boswell [1.36] on a few metals and some alkali halides clearly established that the lattice constant decreases with decreasing particle size. This is further confirmed by numerous subsequent studies. Typical results obtained by Boswell are given in Table 1.6. The decrease in lattice constants with decrease in particle size is consistent with the theory of surface effects in crystals [1.37].

1.3.12 Lattice Constants and Point Defects in Crystals

Lattice parameter determination yields interesting information regarding point defects in crystals. It is well known that the formation of vacancies in metals or Schottky defects in ionic crystals leads to an increase in bulk volume as new atomic layers are formed on the crystal surface. This means that the bulk density (ρ_m) decreases. No such change takes place when Frenkel defects are formed. On the other hand, the existence of pure interstitials results in an increase in bulk density.

The density of a crystal can be calculated from the lattice parameter from the relation:

$$\rho_{\mathrm{x}} = Mn\,/N_{\mathrm{A}}\,a^3, \tag{1.12}$$

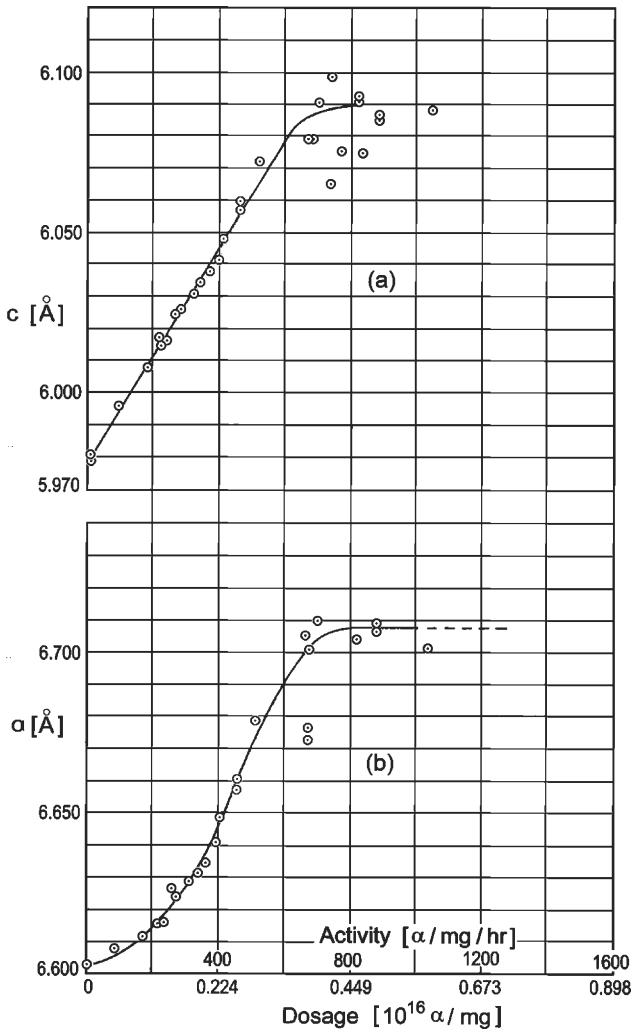

Fig. 1.28. Variation of lattice parameters c and a of zircon with α-activity

where M is the molecular weight, n the number of formula units in the unit cell, N_{A} Avogadro's number and a the lattice constant. ρ_{x} is called the X-ray density or ideal density. Its value is not affected by the presence of a small number of defects. From the above discussion, we have the following relations between ρ_m and ρ_{x}:

Schottky defects $\rho_{\mathrm{m}} < \rho_{\mathrm{x}}$
Frenkel defects $\rho_{\mathrm{m}} = \rho_{\mathrm{x}}$
Interstitials $\rho_{\mathrm{m}} > \rho_{\mathrm{x}}$